*Supporting Information for*

# Amplified emission from halide perovskite quantum dots by exciton–plasmon-coupled energy transfer in the neutral and trion states on gold nanoparticles

Bhagyashree Mahesha Sachith, Yifei Xia, Tianci Wang, Takuya Okamoto, Syoji Ito, Li Wang, Xu Shi, Naoto Tamai, Hiroshi Miyasaka, Hiroaki Misawa, Vasudevanpillai Biju

## EXPERIMENTAL SECTION

### Materials

Methylammonium bromide (MABr, >98.0%), oleic acid, γ-butyrolactone (GBL, >99.0%), dry *N,N*-dimethylformamide (DMF, ≥99.5%), and oleic acid (>85.0%) were from the Tokyo Chemical Industry. 1-Hexadecene (>90.0%), hexadecyl amine (HDA), and dehydrated toluene (>99.5%) were from FUJI-film Wako Pure Chemicals, Japan. $PbBr_2$ (≥98.0%) was from Sigma-Aldrich, Japan. These chemicals were used without further purification.

### Synthesis of $MAPbBr_3$ L-PQDs

The $MAPbBr_3$ L-PQDs were synthesized by the LARP method.[48] Briefly, MABr (0.25 mmol), $PbBr_2$ (0.27 mmol), HDA (0.19 mmol), and oleic acid (80 μL) were mixed in 1 mL of dry DMF by stirring at 60 °C. The precursor solution was injected into 50 mL of toluene (80 °C) with vigorous stirring (350 rpm). The reactants formed a green solution, which gradually turned orange-yellow and became turbid under vigorous stirring for 15 minutes. This sample was centrifuged at 10,000 rpm for 5 min. The PQD residue was redispersed in toluene and used in optical studies.

### Synthesis of $MAPbBr_3$ W-PQDs

The $MAPbBr_3$ W-PQDs were prepared using a modified spray technique.[50] Briefly, MABr (0.5 mmol) and $PbBr_2$ (0.5 mmol) were dissolved in dry DMF (1 mL) to form a precursor solution. This solution was mixed with 1 mL of GBL in a glass vial with a spray cap. This mixture was spray-coated (100 μL/s) onto glass or Au NP substrates (25 °C) under the ambient atmosphere (ca. 65% relative humidity). The distance between the spray bottle and the substrate was

maintained at about 15 cm to achieve uniform microdroplet distribution and uniform-sized PQDs.

## Methods

### Absorption and PL measurements

The diluted L-PQD colloidal solution was characterized using a fluorescence spectrophotometer (Hitachi F-4500, Japan, $\lambda_{ex}$ = 400 nm) and a UV-vis absorption spectrometer (Thermo Scientific Evolution 220). Also, the absorption and PL spectra of Au NP substrates, W-PQD, W-PQD-Au NPs, and L-PQD-Au NPs were measured using these spectrometers.

### X-ray diffraction (XRD) measurements

The powder XRD pattern of the $MAPbBr_3$ L-PQD sample was recorded using an X-ray diffractometer (SmartLab, Rigaku) with a Cu Kα X-ray (λ = 1.54 Å).

### STEM measurements

The STEM samples were prepared by drop-casting the L-PQD colloidal solution or by spraying $MAPbBr_3$ in DMF and GBL onto the STEM Cu100P grids. The STEM samples were dried overnight under a vacuum. The STEM and TEM images were obtained using a STEM (Hitachi, HD-2000) operated at 200 kV.□

### Preparation of Au NP film

A magnetron sputter (MSP-1S, VACUUM DEVICE) with an Au target was operated for 7 s, allowing bluish Au NP formation on glass coverslips (25 × 50 $mm^2$) placed on the sputtering stage.

### Single-particle PL measurements

We used Au NP film on glass coverslips and glass coverslips as PQD substrates. 10 μL of a diluted L-PQD colloidal solution in toluene was drop-casted onto the substrates, overlaid with lens-cleaning paper, and dragged horizontally. W-PQDs were prepared on the substrates by spraying, as discussed above. The PL intensity trajectories of single PQDs were recorded at a frame rate of 15 or 30 ms using an EMCCD (iXon, Andor Technology) camera connected to an inverted optical microscope (IX71, Olympus). The emitted photons were collected using an objective lens (40x, Olympus, NA = 0.60) and filtered through a 480 nm long-pass filter. The samples were excited with a 404 nm CW laser (Thorlabs, 8.5 W $cm^{-2}$). Photon antibunching

measurements were carried out using a PicoQuant single-molecule fluorescence detection system.

**Time-resolved PL measurements**

We recorded the PL decays of PQDs on glass and Au NPs using a time-correlated single-photon counting (TCSPC) assembly composed of an avalanche photodiode (Perkin Elmer, SPCM-AQRH) and a TCSPC module (Becker & Hickl GmbH, SPC-830). The samples were excited with a picosecond (ps) laser (Advanced Laser Systems, 465 nm, 45 ps, 1 MHz). The detection field was restricted by an iris placed in front of the photodetector to collect the PL from single QDs.

**TA measurements**

PQDs on glass or Au NPs were excited with femtosecond (fs) laser pulses (400 nm, 200 μW, 1 kHz) from a Ti:Sapphire laser (Spitfire and Tsunami, Spectra-Physics). The probe-pulse repetition rate was set to 0.5 kHz using a chopper (Model 3501, New Focus, Inc.). Absorption transients were probed by delayed fs white-light continuum pulses generated by focusing the fundamental pulses (800 nm) into a $D_2O$ cell. The probe pulses after passing the sample were detected using a polychromator-CCD camera combination (Spectra Pro-275 and Spec-10, Acton Research Co. and Princeton Instruments). The optical density is defined as $\Delta OD = \log (I_{OFF}/I_{ON})$, where $I_{OFF}$ and $I_{ON}$ are the intensities of probe pulses in the absence and presence of the pump pulse, respectively. The time resolution was 100 fs. All TA measurements were performed at room temperature.

**FDTD Simulations**

Electromagnetic simulations were performed to understand the near-field spectra and the near-field intensity distribution of the Au NP and the PQD on the Au NP using the finite-difference time-domain (FDTD) method (Lumerical, Inc.). The optical parameters of $MAPbBr_3$ were obtained from the literature and experimental data.[60] The FDTD simulations were performed on a discrete, homogeneous, spaced mesh with a mesh size of 0.2 nm, creating the simulation models according to the structures and sizes of the Au NPs and PQDs.

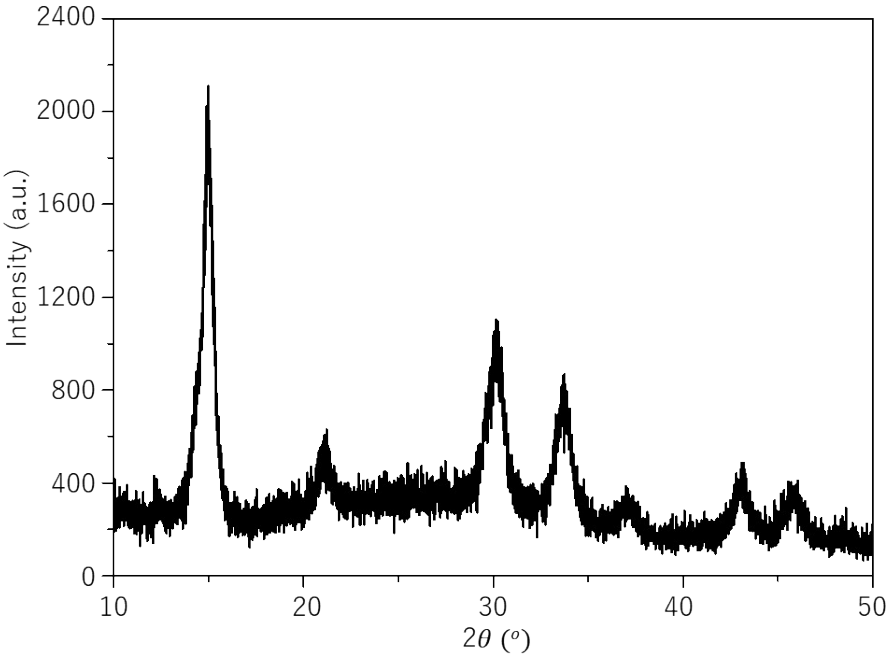


**Figure S1.** The PXRD pattern of $MAPbBr_3$ L-PQDs.

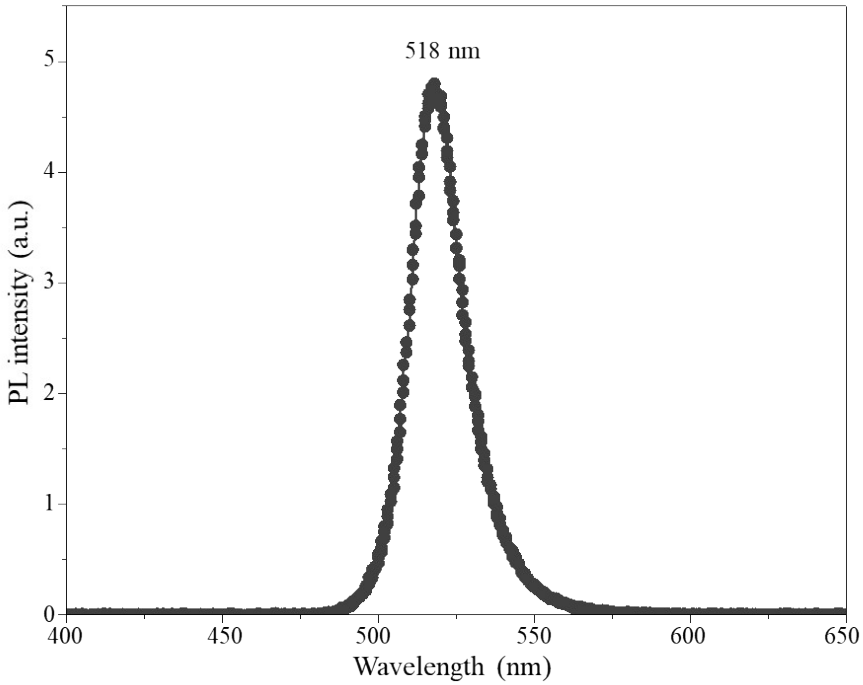


**Figure S2.** A PL spectrum of L-PQDs on a glass substrate ($\lambda_{ex}$ = 404 nm).

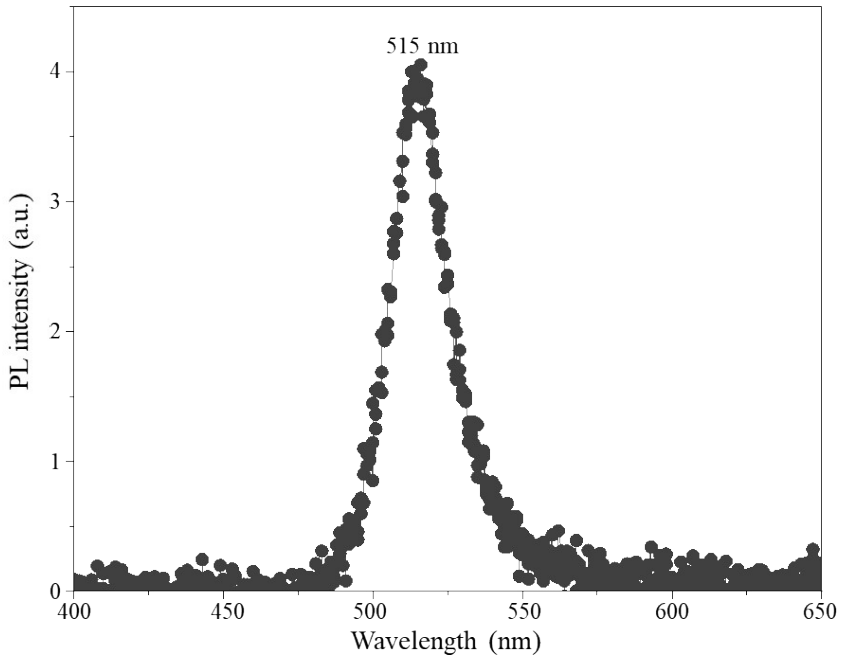


**Figure S3.** A PL spectrum of L-PQDs on Au NPs ($\lambda_{ex}$ = 404 nm).

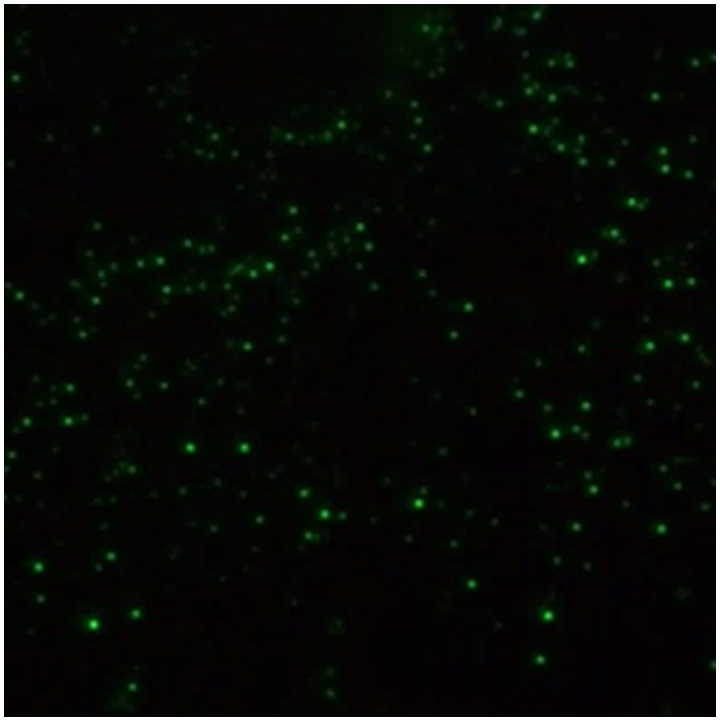

**Figure S4.** A PL image of W-PQDs single particles on a glass substrate (image size: 100 x 100 $\mu m^2$).

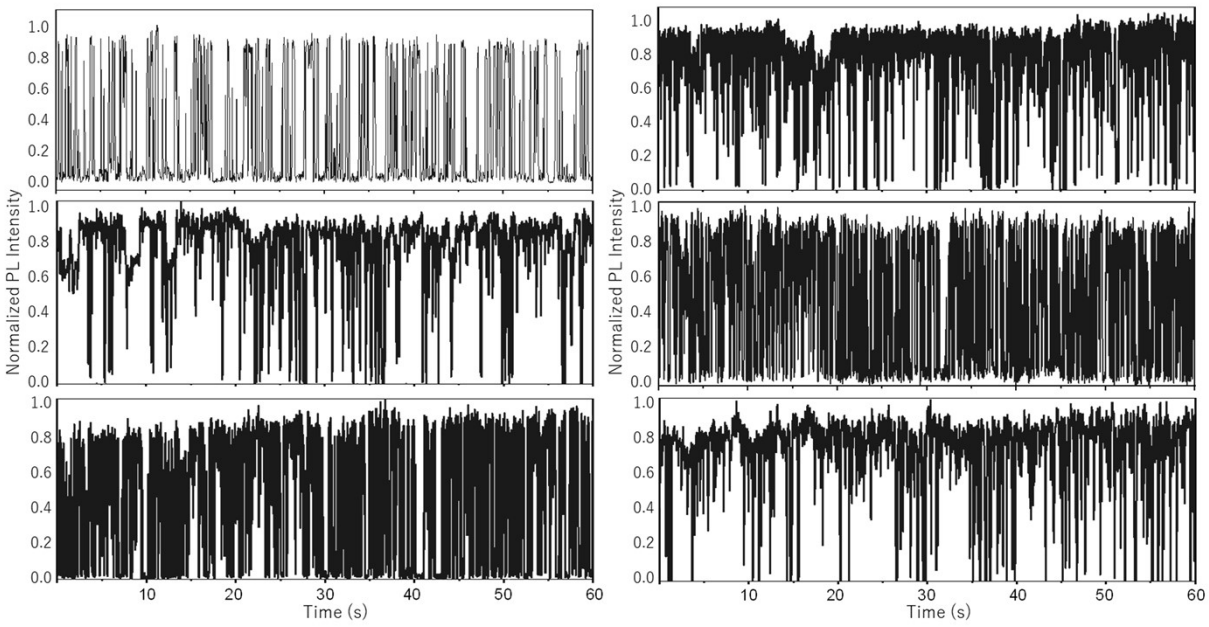


**Figure S5.** PL intensity trajectories of W-PQDs on a glass substrate.

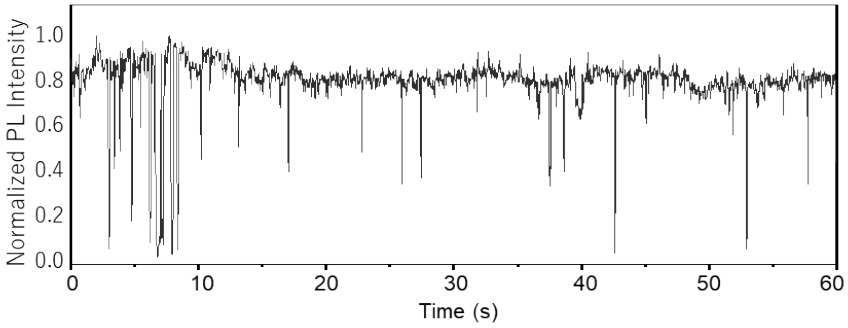


**Figure S6.** A PL intensity trajectory of an L-PQD on an Au NP film.

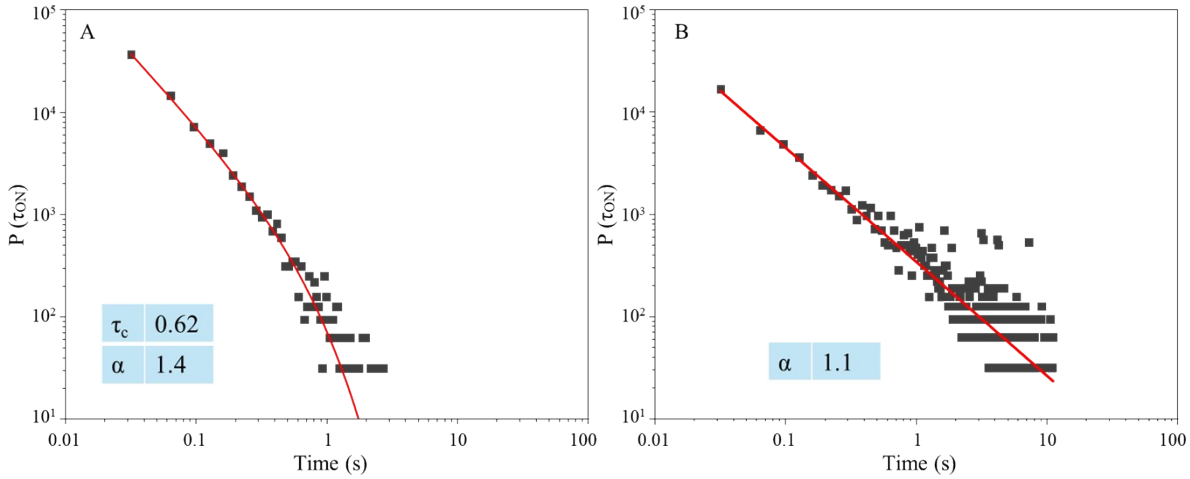


**Figure S7.** Log-log distributions of (A) ON-time and (B) OFF-time probabilities of L-PQDs on Au NPs.

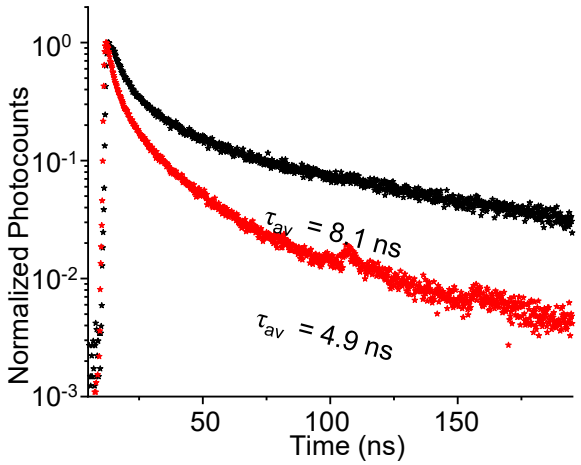


**Figure S8.** PL decay profiles of L-PQDs on (black) glass and (red) an Au NPs film.

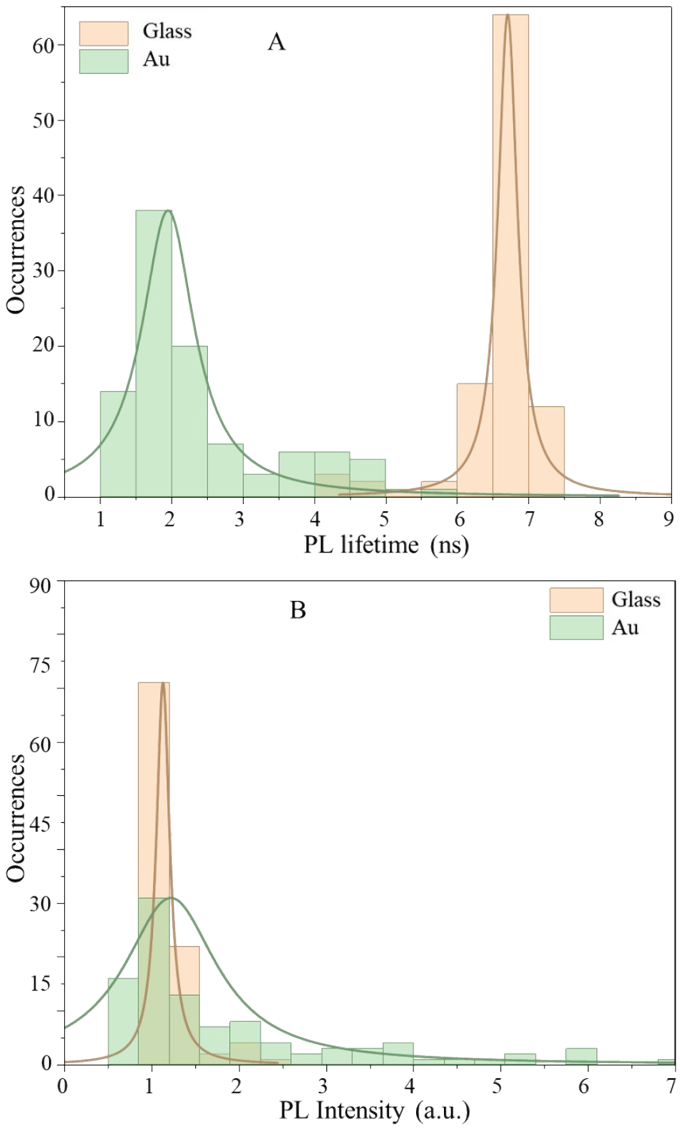


**Figure S9.** PL intensity and lifetime distributions for L-PQDs on glass and Au NPs.

**Table S1**. PL lifetime components of L/W-PQDs on glass/Au NPs.

| Sample | $\tau_1$ (ns) | $\tau_2$ (ns) | $\tau_3$ (ns) |
|---|---|---|---|
| L-PQD/glass | 5.39 (74%) | 16.5 (24.2%) | 30 (1.8%) |
| L-PQD/Au NPs | 3.9 (80%) | 11.1 (18.1%) | 42 (1.1%) |
| W-PQD/glass | 0.49 (0.2%) | 1.78 (96.1%) | 8.69 (3.7%) |
| W-PQD/Au NPs | 0.89 (98%) | 1.1 (2%) | 1 (0%) |

**Table S2**. Biexponentially fitted TA kinetic decay components of W-PQDs on glass/Au NPs.

| Sample | $\tau_1$ (ps) | $\tau_2$ (ps) |
|---|---|---|
| W-PQD/glass | 42 (71%) | 659 (29%) |
| W-PQD/Au NPs | 1.3 (92.2%) | 237.4 (7.8%) |

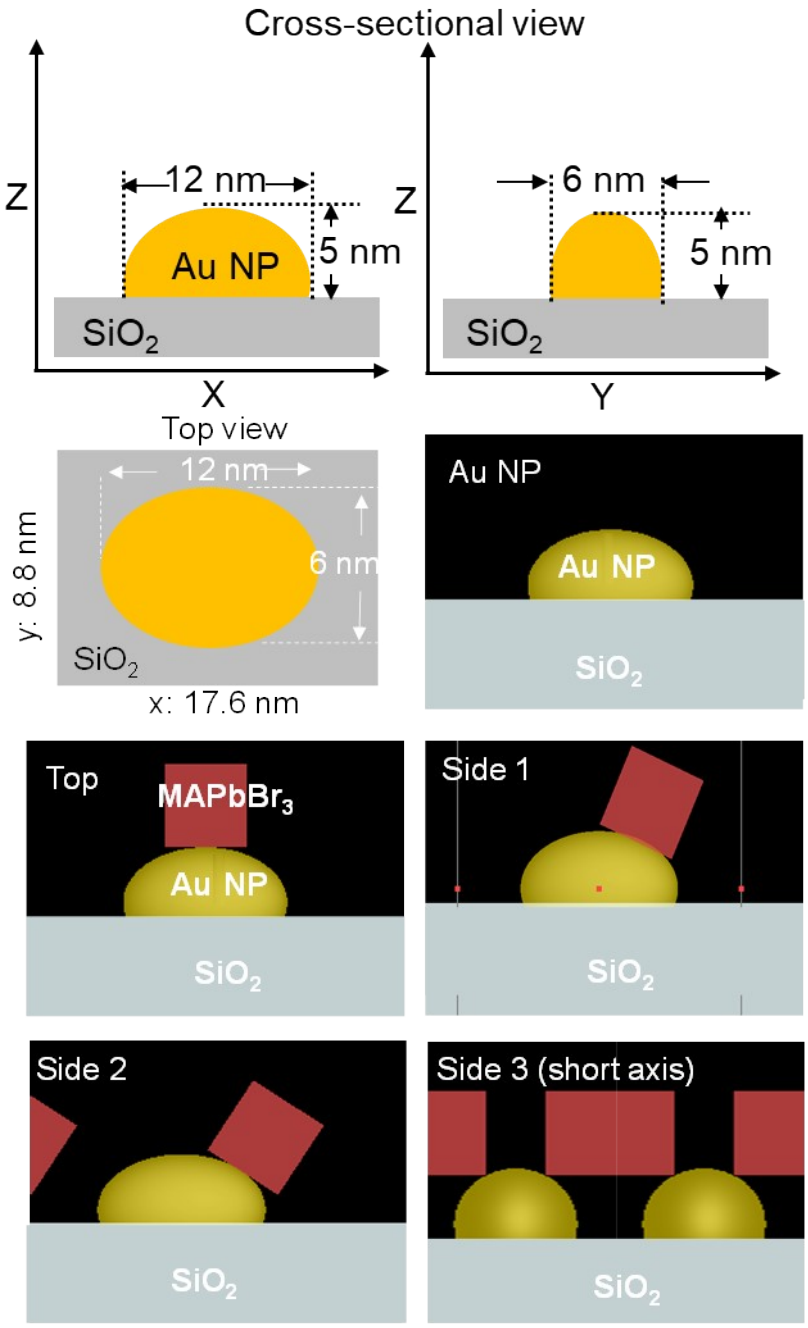


**Figure S10.** Simulation model of Au NP/$MAPbBr_3$ cubic QD. $MAPbBr_3$ QDs are simulated as 6 nm cubes. A periodic boundary condition was applied with a rectangular unit cell (x-period: 17.6 nm; y-period: 8.8 nm), Au-NP surface coverage (36.5% estimated from TEM image), and a mesh size of 0.2 nm. A plane wave light source with circular polarization irradiated Au NP or Au NP/$MAPbBr_3$ cubic QD from the airside.

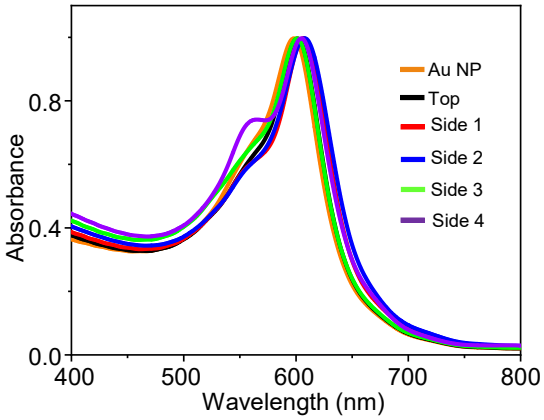


**Figure S11.** Simulated absorption spectra of Au NP (5 nm) and different models of $MAPbBr_3$ and Au NPs.

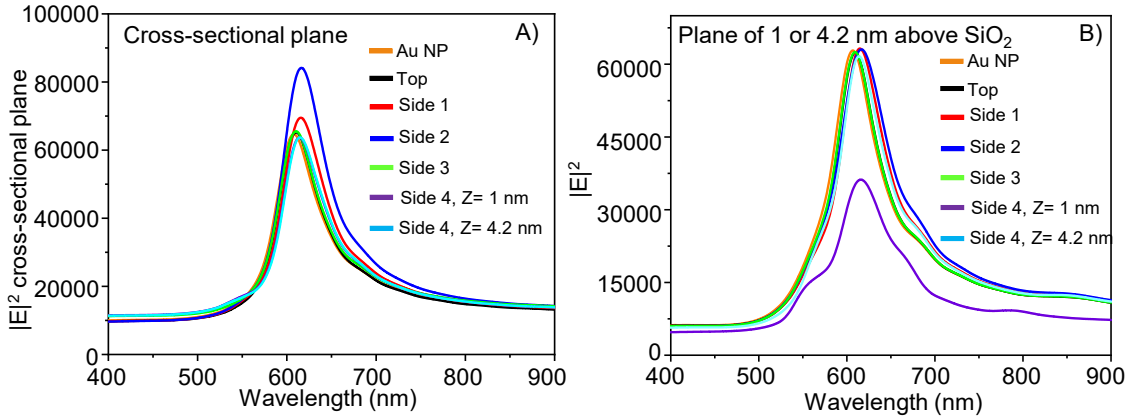


**Figure S12.** Simulated integrated field intensity for (A) cross-sectional planes and (B) the planes 1 or 4.2 nm above $SiO_2$.

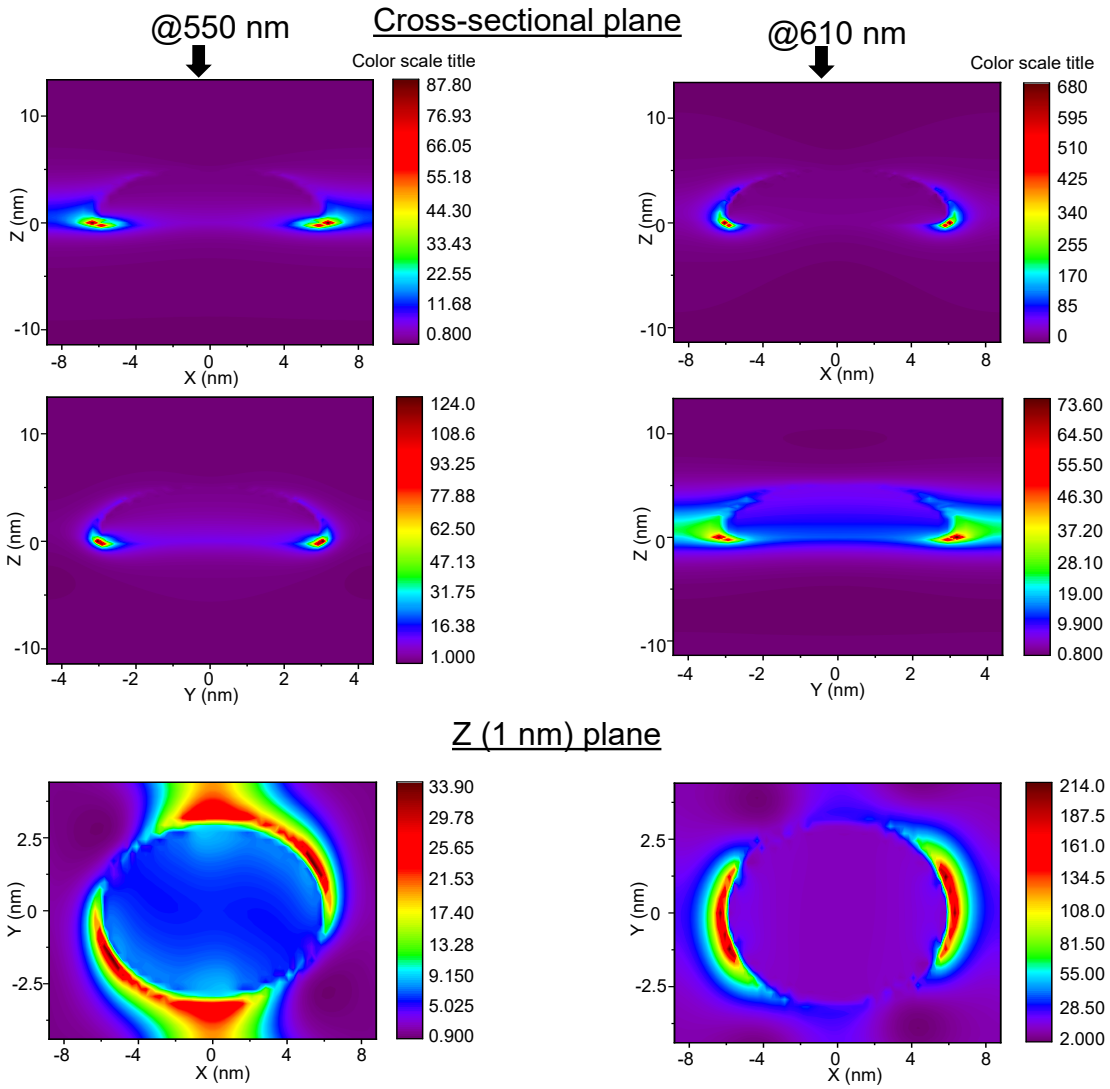


**Figure S13.** Integrated near-field enhancement on Au NP calculated by finite-difference time- FDTD method (cross-sectional plane and Z (1 nm) plane).

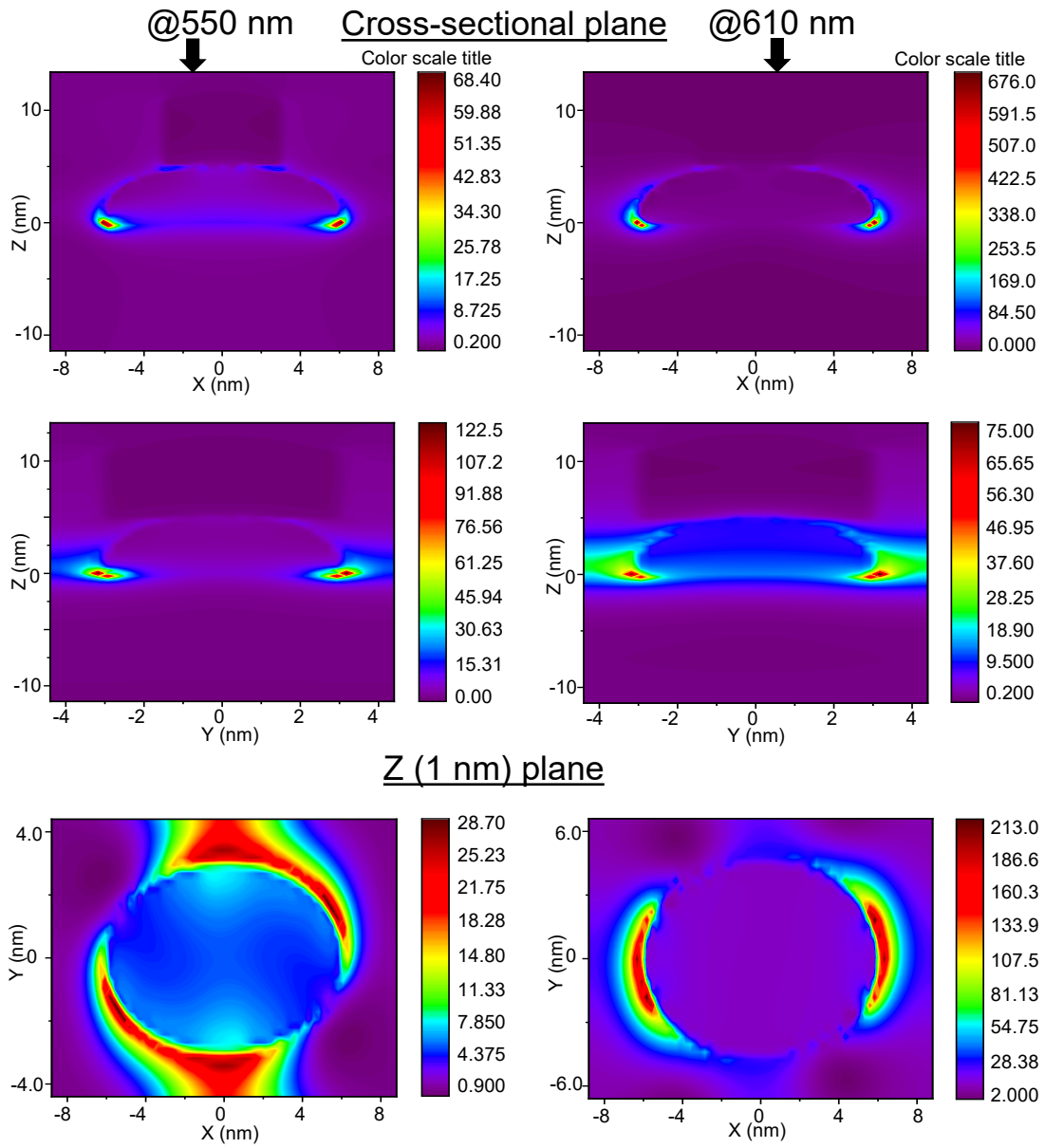


**Figure S14.** Integrated near-field enhancement on W-PQD/Au NP for "top" calculated by finite-difference time- FDTD method (cross-sectional plane and Z (1 nm) plane).

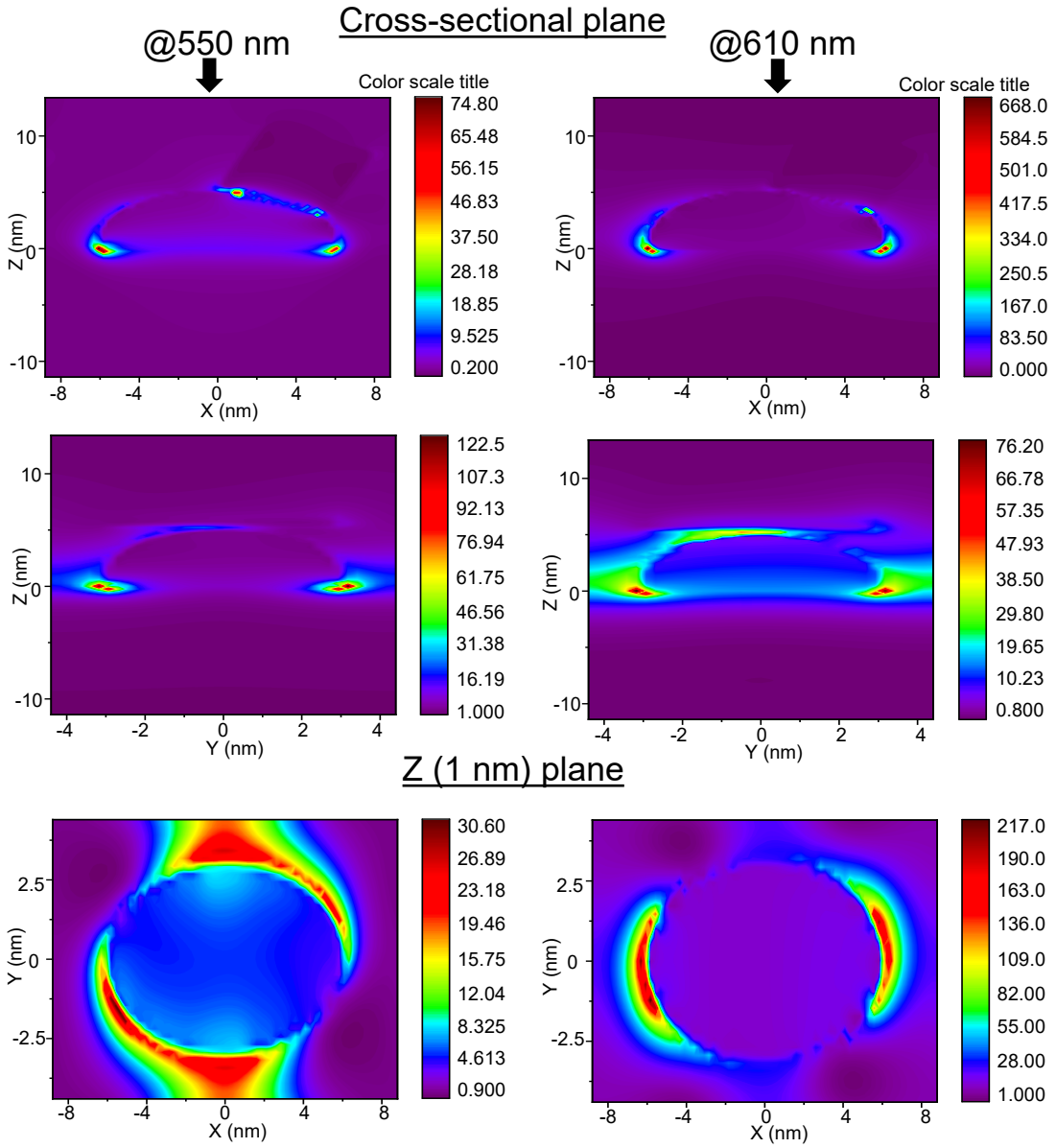


**Figure S15.** Integrated near-field enhancement on W-PQD/Au NP for "side1" calculated by finite-difference time- FDTD method (cross-sectional plane and Z (1 nm) plane).

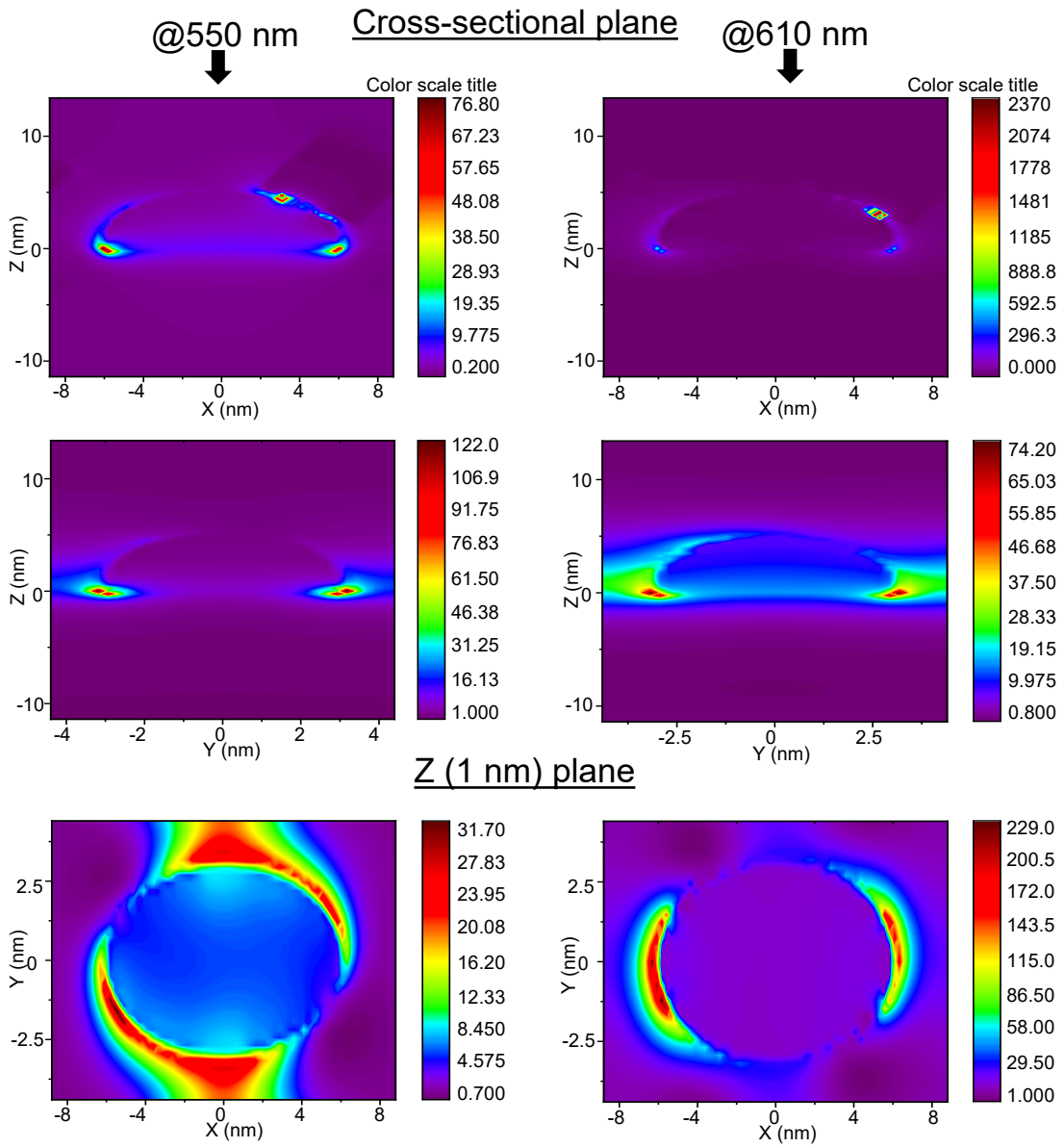


**Figure S16.** Integrated near-field enhancement on W-PQD/Au NP for "side2" calculated by finite-difference time- FDTD method (cross-sectional plane and Z (1 nm) plane).

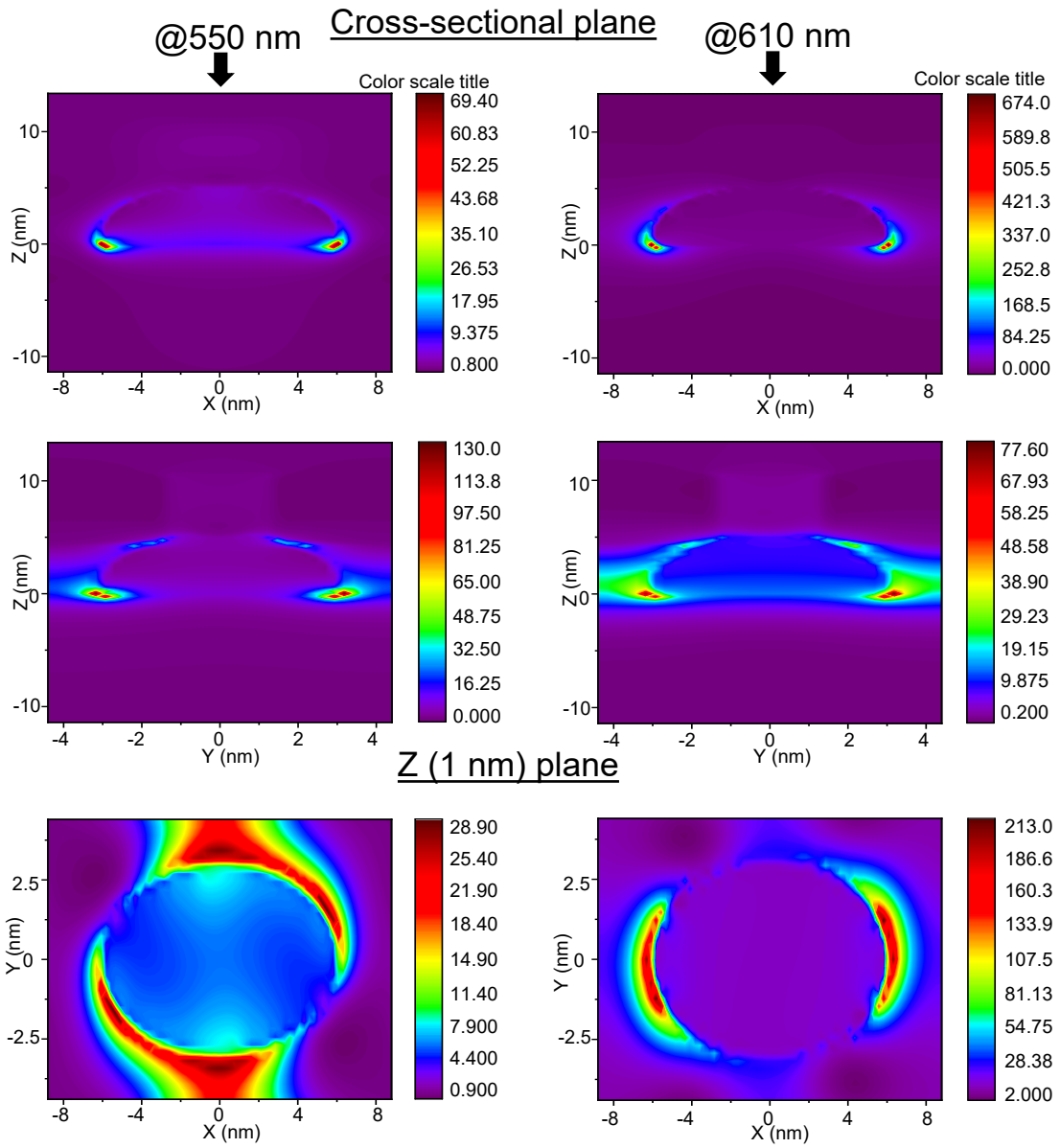


**Figure S17.** Integrated near-field enhancement on W-PQD/Au NP for "side3" calculated by finite-difference time- FDTD method (cross-sectional plane and Z (1 nm) plane).

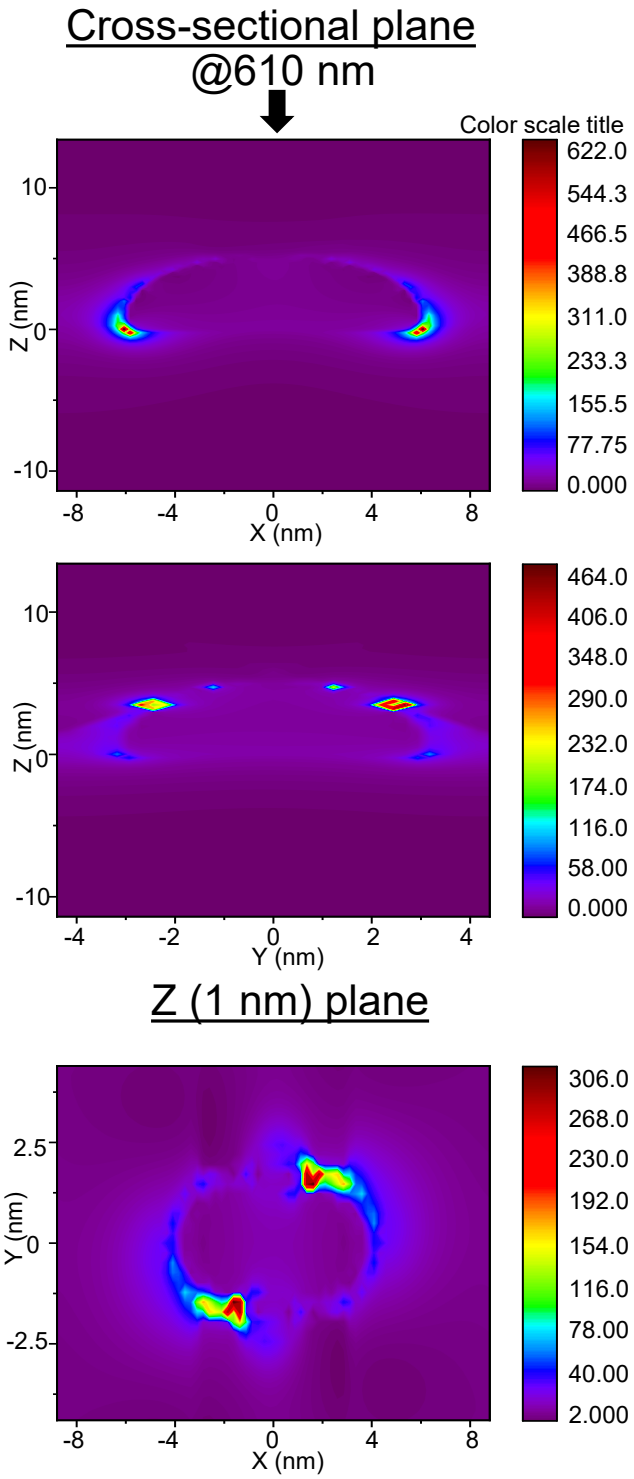


**Figure S18.** Integrated near-field enhancement on W-PQD/Au NP for 'side4' calculated by finite-difference time- FDTD method (cross-sectional plane and Z (4.2 nm) plane). The results for 550 nm are shown in Figure 5.

**Note**

The cited references refer to those in the main text.